

## Response of Global Tropical Cyclone Activity to Increasing CO<sub>2</sub>: Results from Downscaling CMIP6 Models

KERRY EMANUEL

*Lorenz Center, Massachusetts Institute of Technology, Cambridge, Massachusetts*

(Manuscript received 18 May 2020, in final form 16 July 2020)

**ABSTRACT:** Global models comprising the sixth-generation Coupled Climate Model Intercomparison Project (CMIP6) are downscaled using a very high-resolution but simplified coupled atmosphere–ocean tropical cyclone model, as a means of estimating the response of global tropical cyclone activity to increasing greenhouse gases. As with a previous downscaling of CMIP5 models, the results show an increase in both the frequency and severity of tropical cyclones, robust across the models downscaled, in response to increasing greenhouse gases. The increase is strongly weighted to the Northern Hemisphere, and especially noteworthy is a large increase in the higher latitudes of the North Atlantic. Changes are insignificant in the South Pacific across metrics. Although the largest increases in track density are far from land, substantial increases in global landfalling power dissipation are indicated. The incidence of rapid intensification increases rapidly with warming, as predicted by existing theory. Measures of robustness across downscaled climate models are presented, and comparisons to tropical cyclones explicitly simulated in climate models are discussed.

**KEYWORDS:** Atmosphere; Tropical cyclones; Climate change

### 1. Introduction

The cost to society of climate change is driven largely by the costs associated with extreme climate events such as droughts, floods, wildfires, and storms. Slow changes in long-term average conditions, such as annual mean temperature and sea level, can often be accommodated through an equivalently slow adaptation, but adaptation to changes in infrequent events is notoriously flawed and often unduly influenced by politics and special interests (Gaul 2019), making each event disproportionately expensive.

The long-term average annual cost  $C$  of discrete climate events can be defined as the integral of the cost of each event multiplied by the annual probability density of that event, over the whole range of possible costs:

$$C = \int_0^{\infty} c(i)p(i) di, \quad (1)$$

where  $c$  is the cost of an event of intensity  $i$ , and  $p(i)$  is the probability density (probability per unit intensity) associated with that cost.

For extreme events such as tropical cyclones, the cost typically rises steeply and nonlinearly with the intensity of the event, and at the same time the probability of the event drops with its intensity. For this reason, the integral in (1) is usually dominated by costs associated with intensities greater, and possibly much greater, than the intensity associated with the peak of the probability distribution.

This simple point is illustrated in Fig. 1, which is based on damage caused to a portfolio of U.S. properties by 6200

synthetic tropical cyclones making landfall on the U.S. East and Gulf Coasts in two different climate states. These tracks were generated using the technique described in Emanuel et al. (2008) applied to a particular CMIP6-generation climate model, and the damage function and portfolio of property values used by Emanuel et al. (2012). The details of the downscaling methodology are described later in this paper but are not so important here; the point is to illustrate the nature of the problem.

The green curves in Fig. 1 show the annual probability densities of losses as a function of the loss amount; here these are defined as probabilities per unit base 10 log of the cost. The solid curves are for the climate of the late twentieth century, while the dashed curves pertain to the climate of the late twenty-first century under global warming. The most likely event will incur between \$100,000 and \$1,000,000 in losses to this portfolio. The warmer climate has fewer weak events and more strong events; for this illustration the overall frequency is held constant.<sup>1</sup> The violet curves show the probability density multiplied by the cost. The areas under these violet curves are proportional to the total cost. Thus the long-term cost of this hazard is coming from the low-probability, high-intensity tail of the distribution, and the climate shift is causing an appreciable increase in cost even though the shift in the probability distribution is small.

Conversely, *almost no damage is contributed by the median (most frequent) event*. Thus the most frequent question asked by politicians and the media, and many scientists, which is “How will the intensity and frequency of tropical cyclones change?”, is essentially meaningless, because frequency is

 Denotes content that is immediately available upon publication as open access.

Corresponding author: Kerry Emanuel, emanuel@mit.edu

<sup>1</sup>The overall frequency includes some events that cause no damage, so the areas under the probability curves in Fig. 1 are not equal.

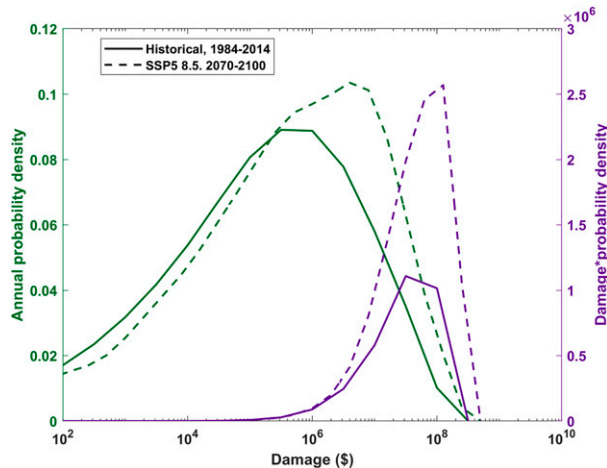


FIG. 1. Annual probability density (green) and damage multiplied by probability density (violet) based on 6200 U.S. landfalling synthetic tropical cyclones downscaled from the MIROC 6 global coupled climate model for each of two periods: 1984–2014 from historical simulations (solid) and 2070–2100 from the Shared Socioeconomic Pathway (SSP) 5 (dashed). The probability density is per unit base 10 log of the damage. The damage is to a portfolio of insured property in the eastern United States and is proportional to the area under the violet curves.

dominated by events that cause very little damage. What we must concern ourselves with is the frequency of the most damaging events. While this illustration pertains only to wind damage, the same is qualitatively the case for water damage.

The climate shift in probability density and damage is not simply a matter of changing frequency and/or intensity but also depends crucially on shifting storm tracks; at the end of the day, all meaningful climate change is local. The damage done by a tropical cyclone is also a strong function of its size, including inner dimensions usually characterized by the radius of maximum winds, and the outer wind field. High category tropical cyclones may have radii of maximum winds as small as 10 km and as large as 100 km while their destructiveness varies between the first and second power of this length scale.<sup>2</sup> Moreover, much of the damage done by tropical cyclones is accomplished by water—specifically, by storm surge, which is sensitive to wind speed, storm size, and translation speed, and by torrential rains, which are sensitive to a variety of storm structural characteristics, intensity, and movement.

For all these reasons, tropical cyclones simulated by most of today’s generation of coupled climate models are unsuitable for direct estimation of tropical cyclone damage. Indeed, the majority of coupled models reviewed by Knutson et al. (2020) have grid spacings of 50 km or greater, whereas numerical

<sup>2</sup> A stationary, steady cyclone just offshore will affect an area proportional to the square of its diameter, while a steady storm moving at constant translation speed will affect a swath proportional to the first power of the diameter, but the duration of winds at fixed points will also depend on storm diameter.

convergence experiments (e.g., Rotunno et al. 2009) suggest that grid spacing on the order of a few kilometers is needed to achieve numerical convergence of azimuthal mean variables.

An alternative to using poorly resolved tropical cyclones from climate models is to downscale such models by embedding within them regional or local models with far greater spatial resolution. A straightforward approach is to drive such embedded high-resolution models with time-evolving boundary conditions supplied from the global models. Examples of this approach are comprehensively reviewed in Knutson et al. (2020). A disadvantage of this approach is that the total number of events simulated is limited by the length of time spanned by the global model simulation and/or by computational cost. Furthermore, in designing the geometries of the high-resolution subdomains, one must take into account the possibility that the regions affected by tropical cyclones might shift with climate change.

For this reason, we adapt the approach described in Emanuel et al. (2008) in which the essential statistical properties of the time-evolving environment are culled from global reanalyses or climate models and used to drive a simple coupled ocean–atmosphere tropical cyclone intensity model along tracks produced by random seeding and a beta-and-advection displacement model. The intensity model has very high spatial resolution in the storm core, owing to the use of an angular momentum radial coordinate, and had been previously shown to produce skillful real-time intensity forecasts (Emanuel and Rappaport 2000). The random seeding is a “natural selection” algorithm; the vast majority of seed disturbances dissipate quickly owing to having been placed in unfavorable environments, leaving a few survivors that had been placed in favorable environments.

There are several advantages to this technique in comparison to conventional downscaling. The use of angular momentum coordinates allows increasing spatial resolution of the storm core as its intensity increases, and thus each storm’s intensity is limited by the physical properties of its environment rather than by numerical resolution. Because the tropical cyclone model is driven by the statistics of the global model or reanalysis, an arbitrarily large number of events can be simulated in a given climate, and the seeding is global so there is no need to preselect subdomains.

Yet there are a number of disadvantages to this approach. The intensity model is axisymmetric, so the dynamical interaction with sheared environments must be parameterized. The shear parameterization used was developed by Emanuel et al. (2004) to optimize the quality of real-time intensity forecasts and is a function of the 250–850-hPa shear magnitude (but not direction) and the saturation deficit of the large-scale environment at 600 hPa. There is no feedback from the simulated cyclones to the regional environment, as there is in conventional downscaling, so the simulation of the extratropical transition of simulated storms is compromised. (The simulated cyclones do respond to the statistics of middle latitude baroclinic systems, but they cannot feedback on such systems.) Finally, in previous work and in what follows here, there has been no attempt to alter the statistics of the random seed disturbances in response to climate change, except that we allow the horizontal scale of the seed disturbances to vary with the

deformation radius based on the large-scale environment. Thus we operate under the assumption that the climatology of tropical cyclones is entirely dictated by the large-scale thermodynamic and kinematic environment and not by the climatology of potential initiating disturbances.

Since most tropical cyclones are triggered by pre-existing disturbances, the notion that cyclone climatology is independent of the climatology of such disturbances is counterintuitive. Yet there is an abundance of evidence that spatial, seasonal, and interannual variability of tropical cyclones is controlled mostly by variations in the large-scale environment. In the first place, genesis potential indices (Gray 1979; DeMaria et al. 2001; Emanuel and Nolan 2004; Emanuel 2010), which are based exclusively on large-scale variables such as potential intensity and wind shear, capture much of the climatology of observed tropical cyclones, including their spatial and seasonal distributions, and interannual variability, at least in the Atlantic region (e.g., Camargo et al. 2007a,b; Bruyère et al. 2012; Camargo et al. 2014). Classical regional downscaling simulations (e.g., Vitart et al. 2007) for the Atlantic region also capture much of the observed interannual variability of tropical cyclone activity when driven by initial and boundary conditions supplied from reanalysis data, but in this case, potential initiating disturbances such as African easterly waves (AEWs) are usually present in the reanalyses and thereby exert an influence on the downscaled tropical cyclones. Yet in one such study (Patricola et al. 2018), AEWs entering the regional domain from the east were artificially suppressed, but the frequency and interannual variability in tropical cyclogenesis was hardly affected. In this case, the AEWs determined the timing and location of genesis events, but not their existence.

The random seeding approach applied here has been shown to capture reasonably well the spatial and seasonal variations of tropical cyclones around the world, and the interannual variability in the Atlantic region, at least as well as classical regional downscaling does (Emanuel et al. 2008). But because the global warming signal is probably not yet detectable in historical tropical cyclone counts (Knutson et al. 2019), there is no way to definitively test this technique's (or any other's) ability to capture the possibly unique character of the global climate change signal. We will return to this point in section 4.

## 2. Methods and data

We use the same downscaling technique originally developed by Emanuel et al. (2006) and Emanuel et al. (2008) and applied to the CMIP5 generation of models by Emanuel (2013). We have made some minor modifications to the technique since its application to CMIP5 models. These include the following:

- Scaling the radii of maximum winds of the seed disturbances by the deformation radius, based on dry stratification along moist adiabats as determined by the environmental temperature at 600 hPa. This causes a modest increase in the average size of simulated tropical cyclones with warming of the free troposphere.

- Slightly modifying the coefficients governing beta drift.
- Calculating the monthly mean ocean mixed layer depths and submixed layer thermal stratification from the global model output rather than from historical climatology; the effect of this is to modestly reduce the number of very intense storms (Emanuel 2015).
- Adding detection of secondary eyewalls that occur in the Coupled Hurricane Intensity Prediction Scheme (CHIPS) model and modifying the canonical radial profiles of wind speed to account for them. This does not affect the global statistics presented here but does affect the calculation of wind speeds at fixed points and thereby, for example, the damage calculations such as those mentioned in the introduction.
- Applying a database of surface roughness over land used to calculate the neutral drag coefficients, replacing the crude parameterization based on topography used before. The new drag coefficients over land are applied to both the CHIPS model and the post-processing algorithms that calculate rainfall. This change does not affect storms over water unless they have previously passed over land.

For the current study, we applied the technique to nine global climate models and to two climate regimes: the period 1850–2014 from historical simulations, and an arbitrary 151-yr period from simulations in which atmospheric CO<sub>2</sub> increases by 1% yr<sup>-1</sup>. In each case, 150 synthetic tracks were generated for each year, yielding 24 750 events for the historical period, and 22 650 events for the increasing CO<sub>2</sub> simulations. The random seeding rate is calibrated for each model to yield an 1850–2014 average annual global frequency of 84 storms, close to the post-1980 observed mean. The global climate models used are listed in Table 1.

## 3. Results

We begin by presenting selected time series of global tropical cyclone activity from the historical period, 1850–2014 and from the 1% yr<sup>-1</sup> CO<sub>2</sub> experiment. The latter is carried out over an arbitrary 151-yr period, but for purposes of comparison we display the results as extending from 1970 to 2120. But note that the measured rate of increase of atmosphere CO<sub>2</sub> has been closer to 0.2% yr<sup>-1</sup>. Our intent here is to examine the general response of global tropical cyclone activity to rising greenhouse gas concentrations, uncomplicated by other climate influences, not to make actual projections. Since the radiative forcing by atmospheric CO<sub>2</sub> over this range of values is nearly proportional to the logarithm of the concentration, we expect trends in global tropical cyclone activity to scale nearly with the annual percentage increase in CO<sub>2</sub> concentration in the absence of other climate forcings.

In the figures that follow, the solid curves show the multimodel means and the shadings show one standard deviation up and down from the mean. Dashed lines indicate the linear regression trends of the multimodel means. Blue represents the historical period and red shows the 1% yr<sup>-1</sup> CO<sub>2</sub> increase experiment.

Figure 2 shows the annual frequency of all tropical cyclones over the globe. The global frequency increases by about 9% over the historical period, 1850–2014, but more rapidly in the

TABLE 1. List of CMIP6 models used in the downscaling of tropical cyclones, including resolution of atmospheric data and principal references.

Institution	Model	Atmospheric resolution <sup>a</sup>	Reference
Canadian Centre for Climate Modeling and Analysis	CanESM5	2.8° × 2.8°	Swart et al. (2019)
Centre National de Recherches Météorologiques	CNRM-CM6-1	1.4° × 1.4°	Voltaire et al. (2019)
National Center for Atmospheric Research	CESM2	1.25° × 0.93°	Danabasoglu et al. (2020)
EC-Earth consortium	EC-Earth3	0.7° × 0.7°	
United Kingdom Met Office Hadley Centre	HadGEM3-GC31-LL	1.25° × 1.88°	Sellar et al. (2020)
Institut Pierre Simon Laplace	IPSL-CM6A-LR	1.25° × 2.5°	Hourdin et al. (2016)
Center for Climate System Research; University of Tokyo; Japan Agency for Marine-Earth Science and Technology; National Institute for Environmental Studies	MIROC6	1.4° × 1.4°	Tatebe et al. (2019)
Max Planck Institute	MPI-ESM1-2-HR	0.94° × 0.94°	Müller et al. (2018)
United Kingdom Met Office	UKESM1-0-LL	1.25° × 1.875°	Sellar et al. (2020)

<sup>a</sup> This is the resolution of the output used to drive the downscaling; it may not correspond exactly with the native resolution of the GCM.

last few decades.<sup>3</sup> Over the 151 years of the increasing CO<sub>2</sub> experiment, the frequency increases by about 25% per doubling of CO<sub>2</sub>. Linear trends and associated *p* values are given for the annual frequency and other tropical cyclone metrics in Table 2.

The previous downscaling of CMIP5 models yielded an increase of roughly 20% per doubling of CO<sub>2</sub>, although those results are not directly comparable to these because the trajectory of CO<sub>2</sub> concentration in the representative concentration pathway (RCP) 8.5 is not the same at that used here.

The green curves in Fig. 2 show the values of a genesis potential index (GPI) summed over the globe (weighted by the cosine of the latitude) for each climate model and then averaged to produce the multimodel mean. The GPI is that of Emanuel (2010) except that the absolute vorticity contribution is capped at  $5 \times 10^{-5} \text{ s}^{-1}$ , following Tippett et al. (2011). This GPI was developed largely independently of the tropical cyclone downscaling algorithm, so this provides a somewhat independent check, although both the CHIPS model and the GPI use potential intensity and a nondimensional measure of midtropospheric specific humidity  $\chi$  as variables.

Figure 3a shows the multimodel mean global frequency of tropical cyclones categorized by Saffir–Simpson intensity and compares them to observations (IBTrACS; Knapp et al. 2010)<sup>4</sup>

<sup>3</sup> This more rapid increase amounts to around 10 events over the period of good global observations, 1980–2018. Given the Poisson random variability of about 9 storms over this period, such a trend would not be statistically detectable at the 5% level, even without considering the effects of natural climate variability on global tropical cyclone frequency.

<sup>4</sup> Data for the North Atlantic and eastern and central North Pacific originated from the National Oceanographic and Atmospheric Administration's National Hurricane Center, and elsewhere from the U.S. Navy's Joint Typhoon Warning Center.

made over the period 1980–2018. Note here that the tropical storm (TS) category only includes synthetic and observed events whose lifetime intensity exceeds 40 kt (1 kt  $\approx 0.51 \text{ m s}^{-1}$ ).

The comparison of the observed frequencies with the events downscaled from the historical period is reasonable, but there are too few category 4 storms and too many category 5 storms. This may reflect a bias in the downscaling methodology or in the climate models, but it is also likely that the observations, which are overwhelmingly based on satellite remote sensing imagery, underestimate the intensity of the most intense

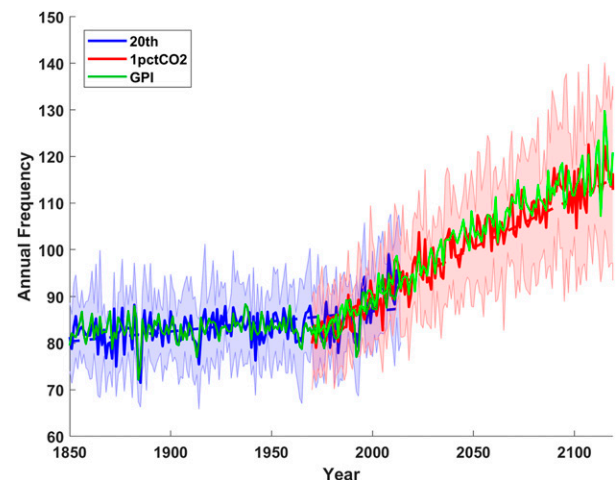


FIG. 2. Annual global frequency of downscaled tropical cyclones. Solid curves represent multimodel means and shading indicates one standard deviation up and down. Dashed lines show linear regression trends. Blue indicates the historical period 1850–2014 while red shows the 1% yr<sup>-1</sup> CO<sub>2</sub> increase experiment arbitrarily beginning in 1970. Green curves show the multimodel mean, globally summed genesis potential index (GPI).

TABLE 2. Historical periods mean and linear trends over the historical period and over the 1% yr<sup>-1</sup> CO<sub>2</sub> increase experiment, expressed in percent change per CO<sub>2</sub> doubling; *p* values are less than 0.01 for all trends except category 2 frequencies, where they are both 0.02.

Quantity	Historical mean	Change over historical period	1% yr <sup>-1</sup> CO <sub>2</sub> (change per doubling)
Overall frequency (yr <sup>-1</sup> )	84	9%	18%
Hurricane frequency (yr <sup>-1</sup> )	57	10%	17%
Category 1 frequency (yr <sup>-1</sup> )	17	5%	8%
Category 2 frequency (yr <sup>-1</sup> )	10	5%	4%
Category 3 frequency (yr <sup>-1</sup> )	10	8%	7%
Category 4 frequency (yr <sup>-1</sup> )	10	13%	26%
Category 5 frequency (yr <sup>-1</sup> )	11	20%	44%
Major hurricanes (yr <sup>-1</sup> )	32	14%	26%
Overall landfall frequency (yr <sup>-1</sup> )	48	7%	17%
Power dissipation index (m <sup>3</sup> s <sup>-2</sup> )	$3.9 \times 10^{12}$	15%	29%
Landfalling power dissipation (m <sup>3</sup> s <sup>-3</sup> )	$3.3 \times 10^{10}$	9%	25%
Radius of maximum winds (km)	59	2%	11%
Outer radius (km)	630	3%	7%

events, shifting them artificially from category 5 to category 4 (Kossin et al. 2013). Figure 3b shows the same comparison but increasing the intensities of the observed storms by 10%. This increase brings the observed and historically simulated Saffir–Simpson categories into much better alignment, though the partitioning between tropical storms and category 1 storms deteriorates, perhaps because of the ambiguity of the Dvorak method when eyes are beginning to form (Olander and Velden 2019). The observed and historically simulated combined numbers of tropical storms and category 1 storms are in very good agreement. Thus it is likely that either the actual storm intensities are underestimated or the simulated storm intensities are overestimated. We note that the 10% adjustment does not improve the agreement in the Atlantic region (not shown), perhaps because storms are better observed there. CO<sub>2</sub>-induced warming brings about increases in the frequency of all categories, but the increases in category 2 and 3 events are small. These are in a flat minimum in the frequency distribution

among categories, so that a shift to higher intensities at constant overall frequency would lead to little change in the frequencies of those categories.

Figure 4 is in the same format as Fig. 2, but shows the evolution over time of the power dissipation index, which is the sum over each track and over all tracks in a given year of the cube of the maximum surface wind. The power dissipation increases at a rate of about 30% per doubling of CO<sub>2</sub>. This is lower than the CMIP5 result (Emanuel 2013) of closer to 40%. Note also, from Table 2, the statistically significant increase of about 15% through the period 1850–2014.

We also consider a landfall power dissipation index, which is the cube of the wind speed at landfall summed over all landfalling events in each year. Here landfall is determined using a  $1/4^\circ \times 1/4^\circ$  bathymetry/topography dataset, and we consider all landfalls, even if a storm makes landfall more than once. Figure 5 and Table 2 show that the multimodel mean landfall power dissipation increases by about 9% over the historical

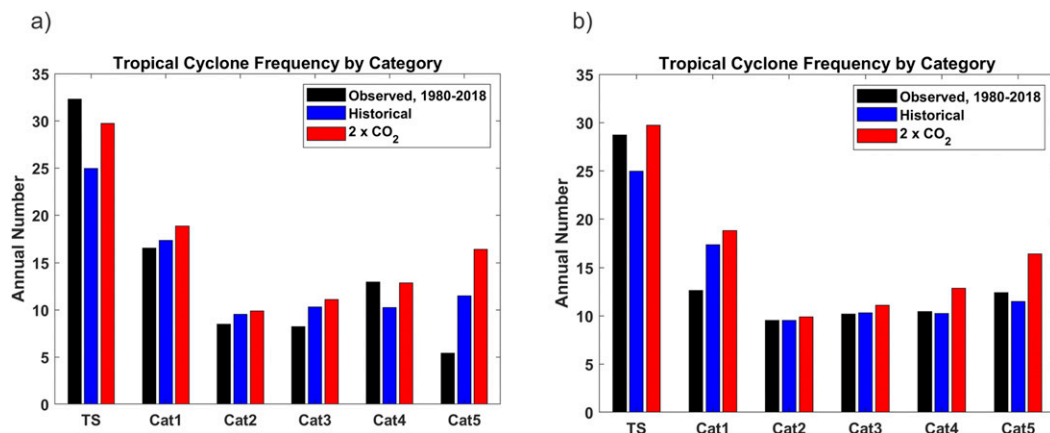


FIG. 3. (a) Global number of tropical cyclones by Saffir–Simpson category of lifetime maximum intensity. Tropical storms here include only events with maximum intensities of at least 40 kt. Black indicates observed (IBTrACS) during the period 1980–2018, while downscaled events are shown in blue for the historical period and red from the linear regressions of trends in the 1% yr<sup>-1</sup> simulations at the time of CO<sub>2</sub> doubling. The downscaled events are multimodel means. (b) As in (a), but observed intensities have been increased by 10%.

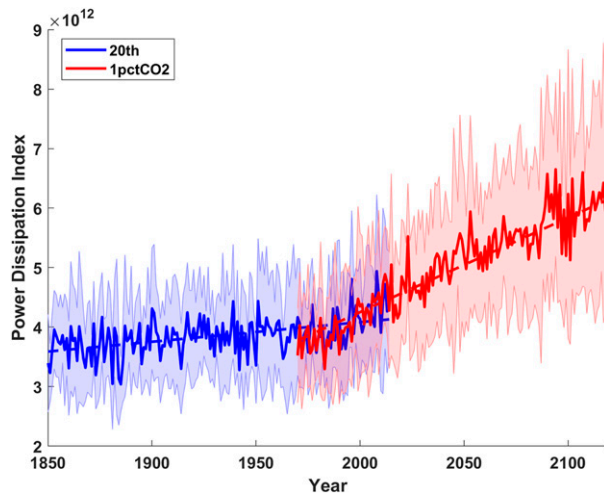


FIG. 4. As in Fig. 2, but showing the power dissipation index.

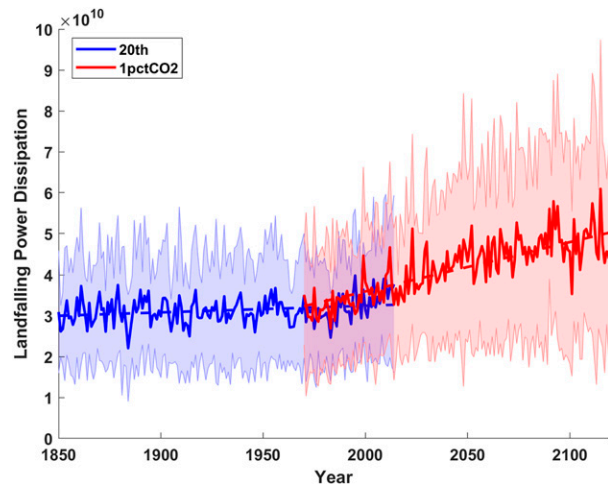


FIG. 5. As in Fig. 2, but showing the landfall power dissipation index.

period and the projected increase is about 25% per doubling of  $\text{CO}_2$ , a bit less than the open-ocean increase in power dissipation.

The spatial patterns of three multimodel mean tropical cyclone metrics and their changes with increasing  $\text{CO}_2$  are shown in Fig. 6. The top row shows genesis density—the number of genesis events per  $1^\circ$  latitude square per year, while the middle row shows the track density and the bottom row shows the power dissipation density. In the case of track density, each track is counted only once in any lat/lon box used to grid the data, whereas the power dissipation is summed over all 2-h points along each track in each box. The left side of Fig. 6 is based on IBTrACS data from 1979 to 2015 while the center column shows multimodel mean quantities from the historical downscaling. The right-hand side of Fig. 6 shows the percentage change between the mean over this historical period and the mean over the  $1\% \text{ yr}^{-1}$  increasing  $\text{CO}_2$  simulations. The change is displayed only where at least 7 of the 9 models agree with each other on the sign of the change.

The historical mean fields in Fig. 6 show some of the same biases noted in the CMIP5 downscaling and also present in the climatologies of storms explicitly simulated in many of these models (e.g., Camargo 2013) and in CMIP6 models (Roberts et al. 2020). There are too many storms in the Southern Hemisphere, including the South Atlantic, and too few tropical cyclones in the eastern North Pacific. Genesis is too active in the central North Pacific, and there are too few storms in the North Atlantic. Some of these biases are also present in tropical cyclones downscaled from climate reanalyses (not shown), so these are probably an artifact of the downscaling technique. It is evident from the track density maps that the downscaled tracks extend somewhat farther poleward than the IBTrACS storm tracks, except in the North Atlantic. This is likely owing to differing conventions on when to terminate tracks of tropical cyclones undergoing extratropical transition. Most forecasting agencies terminate tropical cyclone tracks when the storm is deemed to have become mostly extratropical. Termination of the downscaled tracks, on the other hand, is based only on the

intensity having fallen below a set threshold. Thus we expect that downscaled extratropical transitioning storms will be carried somewhat farther poleward than IBTrACS events.

Turning attention to the percentage changes between the historical to the global warming simulations (right-hand column of Fig. 6), note that there is essentially no change in any metric in the South Pacific, as was the case in downscaling the CMIP5 models. There is little change in the genesis rate in the south Indian Ocean, but the power dissipation increases and the tracks extend somewhat farther poleward, suggesting that the tropical cyclones in this part of the world become more intense and are able to travel farther poleward before dissipating.

The most profound changes occur in the Northern Hemisphere. The genesis maps show a northward expansion of the North Atlantic genesis region and the central and western North Pacific genesis belts. The eastern North Pacific and Arabian Sea genesis regions both expand westward. Partially as a result of these changes in genesis, there are large increases in track density and power dissipation throughout much of the Northern Hemisphere, especially in the central North Pacific and the subtropical to high-latitude North Atlantic. The largest percentage increases are, fortunately, away from land. Especially noteworthy is the large increase in track density in the high latitudes of the North Atlantic, suggesting that the northward expansion of the Atlantic genesis region and the increase in storm intensity there lead to a greater incidence of extratropical transition. This is consistent with recent projections of extratropical transition that suggest increases in the western North Pacific and North Atlantic (Liu et al. 2017; Michaelis and Lackmann 2019).

The large increase in tropical cyclone activity in the Northern Hemisphere relative to the Southern Hemisphere is consistent with explicitly simulated storms in CMIP6 models (Roberts et al. 2020) and the pattern of changes in track density resembles both observed changes over the period 1980–2018 and changes simulated by a suite of high-resolution coupled models over the same period (Murakami et al. 2020), with large increases in the North

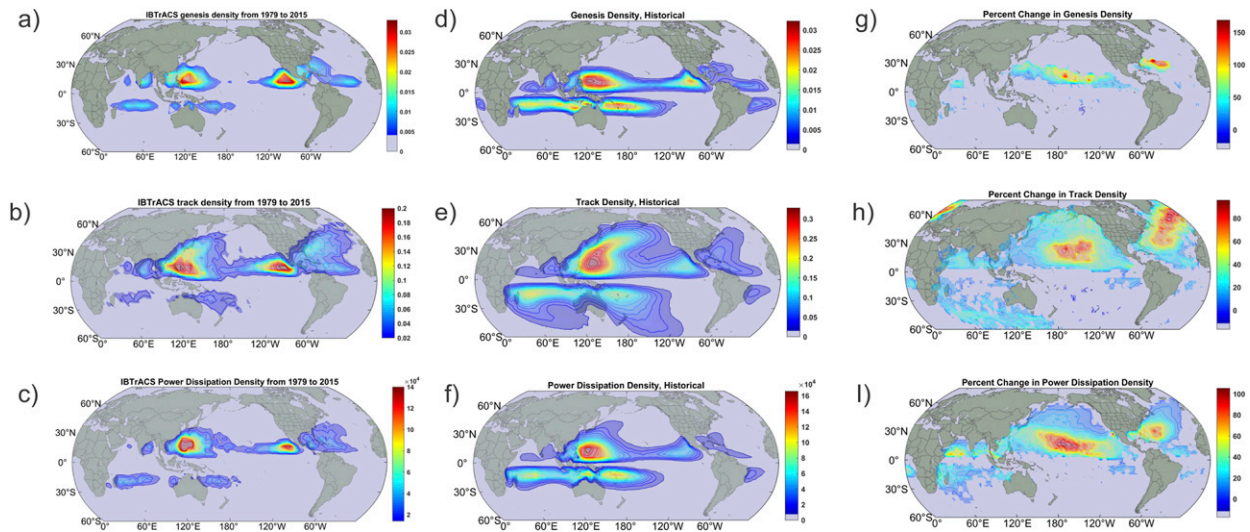


FIG. 6. (top) Genesis density, (middle) track density, and (bottom) power dissipation density (a)–(c) from IBTRACS data, 1979–2015, (d)–(f) the multimodel mean over the historical period, and (g)–(i) the percentage change from the historical period to the mean of the 1%  $\text{yr}^{-1}$  simulation. The changes are only displayed where seven or more of the models agree on the sign of the change.

Atlantic and central North Pacific. But the same models, forced by increasing  $\text{CO}_2$  alone, show decreasing track density in the North Atlantic.

The poleward expansion of both the track and power dissipation density in the Northern Hemisphere and south Indian Ocean is consistent with recent observations of the poleward migration of the latitudes at which tropical cyclones are observed to reach peak intensity (Kossin et al. 2014) and with projected poleward migration in the western North Pacific (Kossin et al. 2016).

In forecasting individual tropical storms, the intensification rate is an important consideration because rapidly intensifying events near the time of landfall can catch forecasters and

emergency managers off guard. Theoretically, intensification rates should scale as the square of the potential intensity, so they are more sensitive to climate change than the intensity itself (Emanuel 2017). Figure 7a shows the base 10 logarithm of the probability densities of the multimodel mean and standard deviation of intensification rates based on 2-hourly fixes of the downscaled tropical cyclones. These probability densities are independent of overall storm frequency. Figure 7b shows the percentage difference between the historical period and the 1%  $\text{yr}^{-1}$  simulations. There are large percentage increases in intensification rates exceeding about  $3 \text{ kt h}^{-1}$ , and this percentage change increases with intensification rate. There is also a smaller increase in extreme dissipation rates, likely

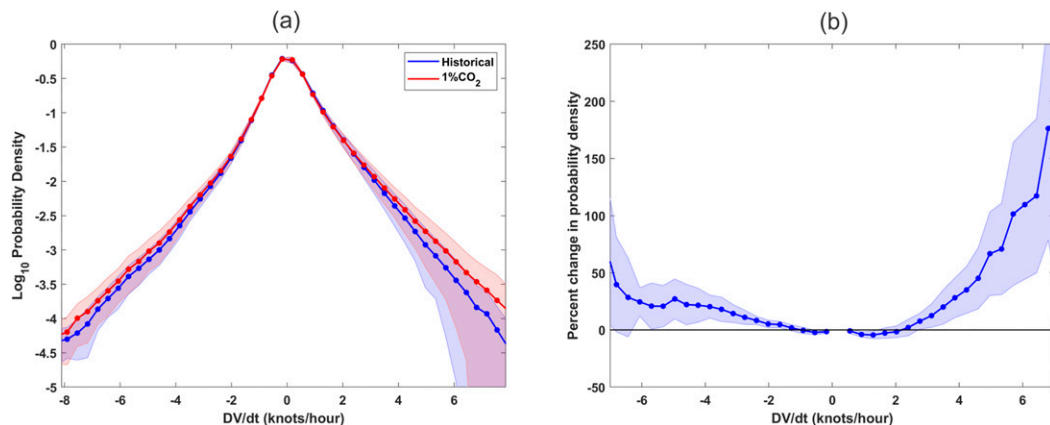


FIG. 7. (a) Base 10 logarithm of the multimodel mean probability density of intensification and dissipation rates of downscaled tropical cyclones over the historical period (blue) and the 1%  $\text{yr}^{-1}$  simulations (red). The shading shows one standard deviation up and down from the mean among the models. (b) Percentage change between the historical and 1%  $\text{yr}^{-1}$  simulations. Shading shows one standard deviation up and down from the mean change among the models.

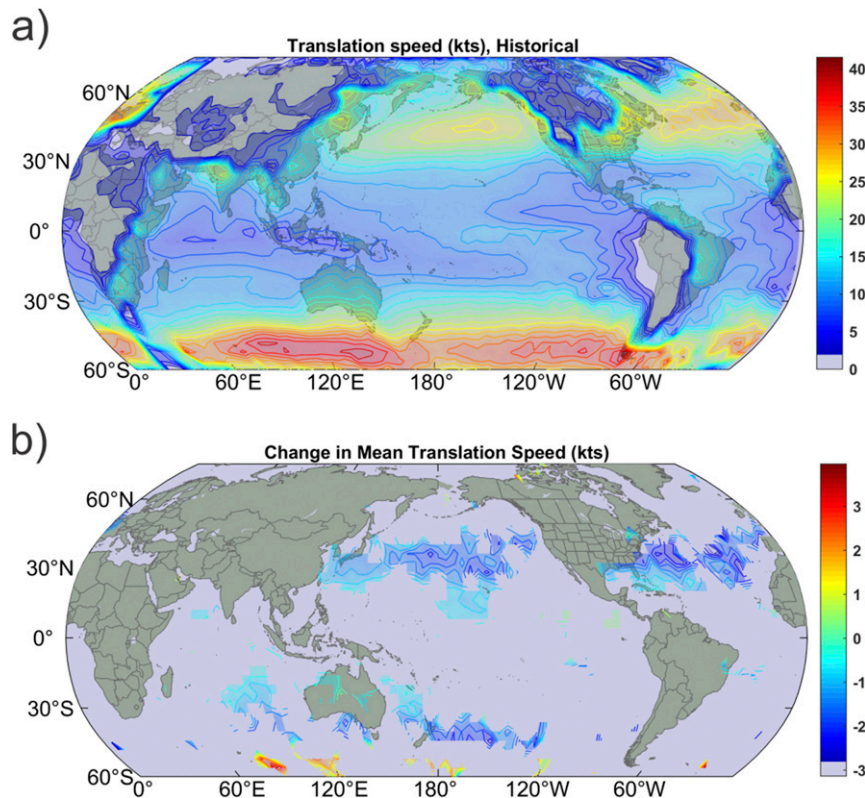


FIG. 8. (a) Multimodel mean translation speed (kt) for the historical period and (b) the change after a doubling of  $\text{CO}_2$ . The latter is displayed only where at least seven of the nine downscaled models agree on the sign of the change.

owing to the faster decay rates of initially more intense storms over land and cold water, because the decay rates scale roughly with the square of the surface wind speed.

The flooding potential, and to some extent the wind damage, caused by tropical cyclones can be strongly affected by their translation speed. Slower moving storms will affect a given region for a longer period, producing more rain and perhaps more wind damage. On the other hand, slow-moving storms are not likely to travel as far inland, sparing regions away from coastlines.

Figure 8 shows the multimodel average translation speed of downscaled tropical cyclones for the historical period (Fig. 8a) and the change in translation speed (Fig. 8b) for a transient doubling of  $\text{CO}_2$ . The latter is displayed only where at least 7 of the 9 GCMs agree on the sign of the change in downscaled translation speed. Remarkably, there is no significant change in translation speed in the deep tropics, but there is a substantial decrease in mean translation speed at the subtropical peripheries of the tropical belt, affecting the U.S. East and Gulf Coasts, the central coast of China, the Korean Peninsula, southern Japan, and Australia. This is perhaps a consequence of the projected poleward expansion of the Hadley circulation. This result can be compared and contrasted to recent global modeling results that show reductions in the subtropics and middle and high latitudes (Yamaguchi et al. 2020) and reductions

primarily in the middle latitudes (Zhang et al. 2020). Lee et al. (2020) used a downscaling method similar to that employed here to examine translations speeds of storms near land, finding a slight reduction.

#### 4. Discussion

##### a. Changes in weak tropical cyclones

As was the case with downscaling the previous (CMIP5) generation of climate models, the results of downscaling nine CMIP6 models show substantial increases in both the intensity and frequency of tropical cyclones as greenhouse gas concentrations increase. The frequency increase is at odds with most (though not all) results from explicit modeling of tropical cyclones. According to a recent and comprehensive review by Knutson et al. (2020), “the vast majority of individual studies (22 out of 27 studies) project a decrease in global TC frequency with greenhouse warming” (p. E306). It is both of inherent and practical interest to discover why these results differ the way they do.

It should first be noted that the great majority of the studies done to date focused on tropical cyclones explicitly simulated in global atmospheric or coupled general circulation models (GCMs), whose effective horizontal grid spacings vary from 14 km to as much as 200 km. Most of these models moderately

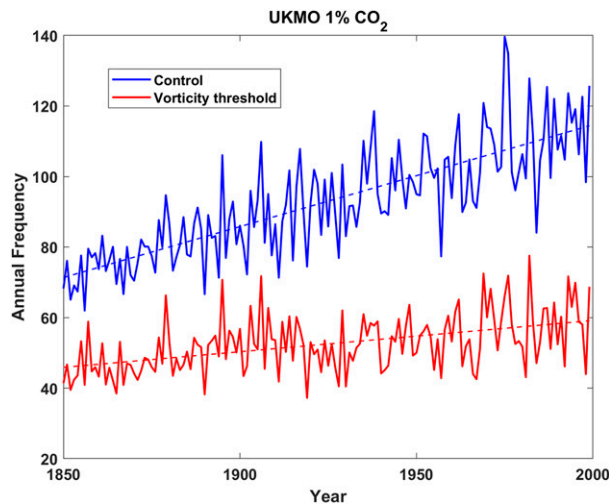


FIG. 9. Time series of annual tropical cyclone counts for the standard downscaling of the UKMO model (blue) and with the imposition of an artificial vorticity threshold (red). Dashed lines show the linear regressions.

to severely underresolve tropical cyclones (see, e.g., Rotunno et al. 2009) and the mesoscale processes observed to be involved in their genesis (e.g., Montgomery and Smith 2012). Tropical cyclones that develop in such models must be detected using an algorithm (e.g., Walsh et al. 2007) and the counts of tropical cyclones are known to be sensitive to how that algorithm is formulated and to model characteristics (Raavi and Walsh 2020).

In particular, climate change may alter the scale and other characteristics of simulated tropical cyclones, pushing events across arbitrary detection thresholds and thereby leading to false trends in counts of weak events. For example, weak tropical cyclone–like disturbances may become broader as the climate warms, as they do in “TC-world” experiments (e.g., Khairoutdinov and Emanuel 2013), and while their circulation may stay the same or even increase, their vorticity may decrease below the imposed vorticity thresholds that are a key feature of most tropical cyclone detection algorithms. Indeed, in their analysis of 850-hPa vorticity in two global models, Sugi et al. (2020) show that as climate warms, the vorticity of disturbances of tropical storm strength decreases proportionally more than does their intensity (cf. their Figs. 2 and 3), suggesting that the pre-tropical cyclone disturbances may be becoming broader.

To test the idea that this could bias trends in explicitly detected cyclones in GCMs, we recalculated time series of downscaled tropical cyclone metrics as before but this time imposing an artificial vorticity-like detection threshold. Specifically, we discarded events whose ratio of maximum circular wind speed to radius of maximum winds is less than  $6 \times 10^{-4} \text{ s}^{-1}$ .

Figure 9 compares the evolution of total tropical cyclone frequency in this modified experiment to the control, for both the historical and increasing  $\text{CO}_2$  simulations of one of the nine models we use in this study. The substantial upward trend of the control frequency in this latter simulation is greatly muted in the modified experiment. In both the control and

the modified experiments, the horizontal scale of the seed disturbances is determined by the local deformation radius, which increases as the climate warms owing to the increase in dry static stability along moist adiabats.

Thus it is possible that the frequency of disturbances detected by a vorticity threshold may decrease relative to the frequency determined by a wind speed threshold. Almost all the GCM-based studies reviewed by Knutson et al. (2020) imposed both vorticity and wind speed detection thresholds, so further research would be necessary to confirm or reject the hypothesis that warming-induced trends in tropical cyclone counts may be negatively biased through the use of a fixed vorticity threshold that does not depend on the climate state.

There are also indications that explicitly simulated tropical cyclones and their sensitivity to climate change may not be robust to changes in model physics or resolution. For example, when the grid spacing of a coupled global climate model was decreased from 50 to 25 km, the sensitivity of tropical cyclone counts to global warming went from negative to neutral (Vecchi et al. 2019). Moreover, in contrast to both observations (Tippett et al. 2011) and the downscaling described here, the relationship between explicit tropical cyclone counts in GCMs and environmental conditions is weak and/or of the wrong character (Camargo et al. 2020).

For these reasons, there is little basis for confidence in the projection by most climate models that overall tropical cyclone frequency will decline. Indeed, 7 of the 11 authors of Knutson et al. (2020) rated confidence in the projection of decreasing tropical cyclone frequency as low-to-medium.

But how believable are the indications of increasing frequency across the spectrum of intensity resulting from this downscaling study (see Fig. 3)? On the one hand, there is excellent correspondence between the downscaled tropical cyclone frequency and the genesis potential index calculated from the raw GCM output (Fig. 2). The GPI was developed and tested largely independently of the development of the downscaling technique, though the variables used in the GPI were selected partly because they are variables that appear naturally in the CHIPS model.<sup>5</sup> Both the CHIPS model and the GPI depend strongly on potential intensity, wind shear, and the midtropospheric dryness parameter  $\chi$  that is based on moist static energy. There is no a priori reason to think that variations in these parameters owing to global climate change would affect tropical cyclones differently from variations owing to spatial, annual and interannual variability, yet both the downscaling and the GPI capture such natural variations quite well. There are, of course, other empirically determined genesis potential indices (e.g., Tippett et al. 2011; Tang and Camargo 2014) and given that these produce different estimates, agreement with the downscaled frequencies presented here would likely be less.

By examining each of the factors that make up the definition of GPI, it is possible to draw some inferences about which

<sup>5</sup> This GPI is also dimensionally correct, yielding genesis number per unit area per unit time. Other genesis indices perform equally well during the historical period but yield very different trends in global warming scenarios (Lee et al. 2020).

environmental factors lead to its increase. The definition of GPI used here is from Emanuel (2010):

$$\text{GPI} \equiv |\eta|^3 \chi^{-4/3} \text{MAX}[(V_{\text{pot}} - 35 \text{ m s}^{-1}), 0]^2 \times (25 \text{ m s}^{-1} + V_{\text{shear}})^{-4}, \quad (2)$$

where  $\eta$  is the absolute vorticity of the 850-hPa flow, capped by  $5 \times 10^{-5} \text{ s}^{-1}$ ,  $V_{\text{pot}}$  is the potential intensity,  $V_{\text{shear}}$  is the magnitude of the 850–250-hPa wind shear, and

$$\chi \equiv \frac{s_b - s_m}{s_0^* - s_b}, \quad (3)$$

where  $s_b$ ,  $s_m$ , and  $s_0^*$  are the moist entropies of the boundary layer and middle troposphere, and the saturation moist entropy of the sea surface, respectively. This is the quantity that is summed over the globe and averaged among the nine models to produce the green curves in Fig. 2. Were it not for that summation, it would be possible to do a linear factor separation of (2) by taking the logarithm of both sides:

$$\begin{aligned} \log(\text{GPI}) &= 3 \log(|\eta|) - \frac{4}{3} \log(\chi) \\ &+ 2 \log\{\text{MAX}[(V_{\text{pot}} - 35 \text{ m s}^{-1}), 1]\} \\ &- 4 \log(25 \text{ m s}^{-1} + V_{\text{shear}}). \end{aligned} \quad (4)$$

Unfortunately, the summation over the globe and the averaging among the nine models does not allow this: The logarithm of the summed, averaged value of GPI given by (2) is not equal to the summed, averaged value of the logarithm of GPI. Since the tuning of the coefficients in (2) was done by matching summed GPI to observations, one cannot willy-nilly use (4) instead of (3) as the working definition of the GPI without retuning. Since that retuning is beyond the scope of this study, we attempt to use (4) anyway, using the summed, averaged quantities (GPI,  $\eta$ , etc.) before taking their logarithms.

Figure 10 shows, for the 1% per year increasing  $\text{CO}_2$  experiment, the evolution with time of the terms in (4), where it is understood that the quantities have first been summed and then averaged among the four models. To avoid extratropical influences, we zero each individual term wherever the potential intensity is  $35 \text{ m s}^{-1}$  or less, and each curve is relative to the initial value of the quantity in question.

The black curve shows the sum of the terms whereas the green curve is the logarithm of the actual GPI; the mismatch between these two curves reflects the problems alluded to above. But for what it is worth, one sees that the potential intensity and saturation deficit are the dominant terms and work in opposing directions. The negative contribution of the saturation deficit  $\chi$  is consistent with the results of Emanuel et al. (2008) and Lee et al. (2020) and suggest that the main break on increasing tropical cyclone frequency in a warming climate is the increasing saturation deficit of the middle troposphere. The vorticity and shear contributions are smaller, but both terms act to increase the GPI trend.

To the extent that the GPI reflects the physics of the downscaled tropical cyclones, we would infer that increasing potential intensity is the most important contributor to increasing cyclone frequency, with small additional contributions

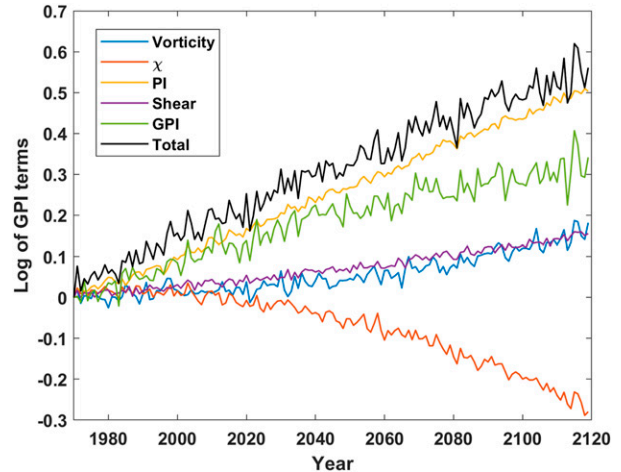


FIG. 10. The terms on the right side of (4); respectively vorticity,  $\chi$ , potential intensity (PI), and shear. The black curve shows their sum while the green curve shows the logarithm of the actual GPI. Each quantity is relative to its initial value.

from decreasing shear and increasing vorticity (likely reflecting the poleward migration of genesis regions). Increasing saturation deficit works in the opposite direction, acting to decrease storm frequency.

It should be noted, however, that changing the exponent of  $\chi$  in (2) to  $-2$  changes the sign of the net response of the GPI to increasing  $\text{CO}_2$  concentration while not strongly degrading the fit to observed variability, so the good fit to the downscaled frequencies is somewhat coincidental. Thus the agreement between the downscaled frequencies and the GPI should not be interpreted as strong evidence for the correctness of either.

Returning to the downscaled tropical cyclones, their rate of genesis varies directly with the specified seeding rate, which is held constant across the globe, seasonally, interannually, and with global climate change. Arguments have been made that this seeding rate should decline as the globe warms (Sugi et al. 2020). Yet the strong spatial, seasonal, and interannual variation of potential initiating disturbances in the current climate does not seem to preclude the ability of either the GPI or the downsampling from capturing major features of natural tropical cyclone variability (Camargo et al. 2007a; Emanuel et al. 2008). Moreover, Patricola et al. (2018) showed that suppressing African easterly waves, a prominent catalyst for North Atlantic hurricanes, did not change the level of tropical cyclone activity in a regional tropical North Atlantic model, although the waves did determine the location and timing of genesis events. Thus the seed disturbances, in this case, did not control the level of tropical cyclone activity.

A more serious deficiency of the downscaling method applied here is that there is no feedback whatsoever between the downscaled tropical cyclones and the large-scale environment that is driving them. Even regional downscaling models, such as that used by Patricola et al. (2018), can simulate some regional feedbacks of cyclone activity within the regional model itself, although they cannot influence the global model in which the regional model is embedded.

There are two known feedback mechanisms by which current tropical cyclone activity can potentially influence future activity through modification of their large-scale environment. The first acts primarily through the ocean: Tropical cyclones cool the sea surface by mixing warmer surface waters with cooler water below the mixed layer (Leipper 1967; Price 1981) and subsequent reheating of the cold wakes leads to a net export of heat away from the affected region (Emanuel 2001; Fedorov et al. 2010). This has the negative feedback of cooling the ocean in tropical cyclone regions, reducing the genesis potential there, but it may lead to increases in genesis in marginal regions outside the main tropical cyclone belts.

A second negative feedback acts through the atmosphere: It is the profound drying of the atmosphere that occurs with any form of aggregation of convection (Bretherton and Khairoutdinov 2004; Wing et al. 2017). This will greatly increase the inhibition to tropical cyclogenesis represented in the GPI by the  $\chi$  parameter and known to strongly affect the genesis rates in the downscaling technique applied here (Emanuel et al. 2008).

Both these mechanisms are, in principle, operating in fully coupled GCMs. To the extent that the large-scale fields are affected by these feedbacks in the GCMs used here, they will also decrease the number of downscaled genesis events, but owing to the severe underresolution of tropical cyclones in most GCMs, these negative feedbacks may be strongly muted.

But there are now some global coupled models with resolutions high enough to capture most of the full spectrum of tropical cyclone numbers and intensities. One such model, the Model for Prediction across Scales–Atmosphere (MPAS-A), was employed by Michaelis and Lackmann (2019) to make global projections of the response of tropical cyclone activity to global warming using a 15-km grid over the whole of the Northern Hemisphere. Notably, they used a cyclone detection algorithm based on sea level pressure anomalies with no vorticity threshold. They found increasing tropical cyclone frequency in the Northern Hemisphere, especially in the Atlantic.

Another high-resolution global coupled model is the NOAA Geophysical Fluid Dynamics Laboratory (GFDL) high atmospheric resolution version of the Forecast-oriented Low Ocean Resolution version of the GFDL global climate model (HiFLOR; Murakami et al. 2015). With an effective grid spacing of about 25 km, this model explicitly simulates high-intensity tropical cyclones (Vecchi et al. 2019). Climate sensitivity experiments with HiFLOR show that increasing CO<sub>2</sub> concentrations leads to a statistically insignificant change in global tropical cyclone counts but a substantial increase in high intensity events (Vecchi et al. 2019). We downscaled 200 events globally per year for 200 years of HiFLOR simulations in two different climates: the climate of the late twentieth century and a climate representing increased CO<sub>2</sub> concentrations. In the former, a single year representing atmospheric greenhouse and aerosol conditions in the year 1990 was repeated over 300 years; we used the last 200 years in the downscaling. The warming experiment starts at year 100 of the control simulation and increases CO<sub>2</sub> at the rate of 1% per year until a doubling has been reached after 70 years; thereafter the CO<sub>2</sub> concentration remains fixed for another 230 years. We use the last 200 years of this simulation. Details may be found in Irvine et al. (2019).

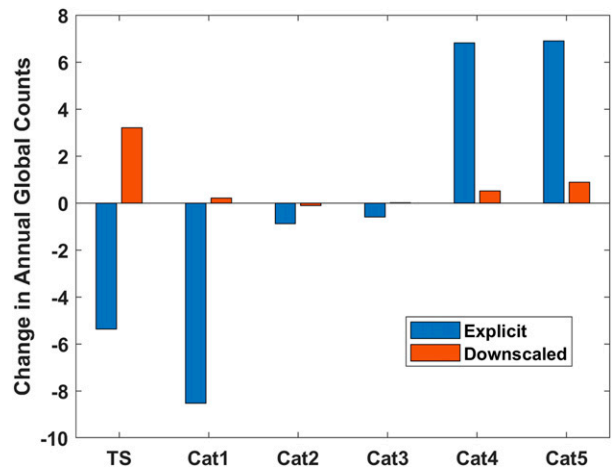


FIG. 11. Change in the annual global frequency of tropical cyclones of six Saffir–Simpson categories. The blue bars show changes in explicitly simulated tropical cyclones in the HiFLOR model, and the red bars show changes in events downscaled from HiFLOR.

Figure 11 shows changes in global counts of tropical cyclones in each Saffir–Simpson category. Note that the HiFLOR model produces about 90 tropical storms per year globally, close to the observed frequency, while the downscaled results have been calibrated to an annual frequency of 84 events in the twentieth century. The distribution across categories of the response of the downscaled tropical cyclones to doubling CO<sub>2</sub> is consistent with that resulting from downscaling of the CMIP6 models (see Fig. 2) but substantially muted in comparison. At the same time, there are substantial increases in the explicitly simulated high intensity (category 4–5) tropical cyclones in HiFLOR, while the number of weak events (tropical storms and category 1 hurricanes) decreases. We speculate that the increase in explicitly simulated intense storm activity in HiFLOR may have led to the aforementioned negative feedbacks, which muted the response of the downscaled storms.

In the author’s opinion, the limitations of CMIP6 model simulations of tropical cyclones preclude any robust projection of the response of weak tropical cyclone activity to global warming, either from their explicitly simulated storms or from events downscaled from their output.

#### b. Changes in high-intensity tropical cyclones

In contrast to the case of marginal storms, detection of cyclones in GCMs becomes less of an issue for intense storms, particularly in the case of high-resolution models that can simulate the full intensity spectrum. Perhaps for this reason, there is much better agreement on projected changes in intense (category 4–5) tropical cyclones, both among the explicitly simulated storms and between them and the downscaled storms [see Fig. 2c herein and compare to Fig. 2a of Knutson et al. (2020)].

### 5. Summary

The application of a downscaling technique to nine CMIP6-generation climate models suggests potentially large increases in various measures of tropical cyclone activity in response to

anthropogenic climate change, particularly in the Northern Hemisphere. These results are broadly consistent with those from downscaling CMIP5 models (Emanuel 2013).

As reviewed by Knutson et al. (2020), there is a moderately strong consensus on an increase in high intensity tropical cyclones and in tropical cyclone rainfall. There is little agreement on how the frequency of weak storms might change, but with the possible exception of rainfall, these are of little consequence. The fact that most explicit modeling studies agree that tropical cyclone frequency will decrease with climate warming may be an artifact of low resolution and the use of non-climate-dependent detection thresholds. Their agreement with each other is only prima facie evidence of robustness of the trend. In the author's opinion, though, the increases in overall tropical cyclone frequency predicted by our downscaling would be muted and perhaps even eliminated by feedbacks from the cyclones to their large-scale environment in two-way coupled simulations that adequately resolve tropical cyclones.

The large increase in the probability of rapid intensification rates is perhaps one of the more worrying aspects of the effect of climate change on tropical cyclones. Given the level of uncertainty in contemporary tropical cyclone intensity forecasts, increasing rates of intensification increase the chances of surprises (Emanuel 2017).

Consistent with some observational studies (Kossin 2018), there is a robust projected decrease in tropical cyclone translation speed in the subtropics, although not in the deep tropics. This may increase the probability of stalling storms, such as Harvey of 2017 and Dorian of 2019. These storms can be especially destructive because of prolonged rain and/or wind.

While the jury may still be out on the effects of climate change on the incidence of weak storms, the growing consensus on substantial increases in high-intensity storms and rainfall paints a robust picture of increasing tropical cyclone risk as the climate continues to warm.

*Acknowledgments.* The author is grateful for the support from the National Science Foundation under Grant ICER-1854929. CMIP6 climate model data was downloaded from a website operated by the Earth System Grid Federation. The author thanks Suzana Camargo and two anonymous reviewers for very helpful suggestions.

*Data availability statement.* The downscaled tropical cyclone data used in this study are freely available from the author for research purposes only. Recipients will be asked to sign and return a data non-redistribution agreement.

## REFERENCES

- Bretherton, C. S., and M. F. Khairoutdinov, 2004: Convective self-aggregation in large cloud-resolving model simulations of radiative convective equilibrium. *26th Conf. on Hurricanes and Tropical Meteorology*, Miami, FL, Amer. Meteor. Soc., 12B.4, [https://ams.confex.com/ams/26HURR/techprogram/paper\\_76059.htm](https://ams.confex.com/ams/26HURR/techprogram/paper_76059.htm).
- Bruyère, C. L., G. J. Holland, and E. Towler, 2012: Investigating the use of a genesis potential index for tropical cyclones in the North Atlantic basin. *J. Climate*, **25**, 8611–8626, <https://doi.org/10.1175/JCLI-D-11-00619.1>.
- Camargo, S. J., 2013: Global and regional aspects of tropical cyclone activity in the CMIP5 models. *J. Climate*, **26**, 9880–9902, <https://doi.org/10.1175/JCLI-D-12-00549.1>.
- , K. A. Emanuel, and A. H. Sobel, 2007a: Use of a genesis potential index to diagnose ENSO effects on tropical cyclone genesis. *J. Climate*, **20**, 4819–4834, <https://doi.org/10.1175/JCLI4282.1>.
- , A. H. Sobel, A. G. Barnston, and K. A. Emanuel, 2007b: Tropical cyclone genesis potential index in climate models. *Tellus*, **59A**, 428–443, <https://doi.org/10.1111/j.1600-0870.2007.00238.x>.
- , M. K. Tippett, A. H. Sobel, G. A. Vecchi, and M. Zhao, 2014: Testing the performance of tropical cyclone genesis indices in future climates using the HIRAM model. *J. Climate*, **27**, 9171–9196, <https://doi.org/10.1175/JCLI-D-13-00505.1>.
- , and Coauthors, 2020: Characteristics of model tropical cyclone climatologies and the large-scale environment. *J. Climate*, **33**, 4463–4487, <https://doi.org/10.1175/JCLI-D-19-0500.1>.
- Danabasoglu, G., and Coauthors, 2020: The Community Earth System Model version 2 (CESM2). *J. Adv. Model. Earth Syst.*, **12**, e2019MS001916, <https://doi.org/10.1029/2019ms001916>.
- DeMaria, M., J. A. Knaff, and B. H. Connell, 2001: A tropical cyclone genesis parameter for the tropical Atlantic. *Wea. Forecasting*, **16**, 219–233, [https://doi.org/10.1175/1520-0434\(2001\)016<0219:ATCGPF>2.0.CO;2](https://doi.org/10.1175/1520-0434(2001)016<0219:ATCGPF>2.0.CO;2).
- Emanuel, K. A., 2001: Contribution of tropical cyclones to meridional heat transport by the oceans. *J. Geophys. Res.*, **106**, 14 771–714 782, <https://doi.org/10.1029/2000JD900641>.
- , 2010: Tropical cyclone activity downscaled from NOAA-CIRES reanalysis, 1908–1958. *J. Adv. Model. Earth Syst.*, **2**, <https://doi.org/10.3894/JAMES.2010.2.1>.
- , 2013: Downscaling CMIP5 climate models shows increased tropical cyclone activity over the 21st century. *Proc. Natl. Acad. Sci. USA*, **110**, 12 219–12 224, <https://doi.org/10.1073/pnas.1301293110>.
- , 2015: Effect of upper-ocean evolution on projected trends in tropical cyclone activity. *J. Climate*, **28**, 8165–8170, <https://doi.org/10.1175/JCLI-D-15-0401.1>.
- , 2017: Will global warming make hurricane forecasting more difficult? *Bull. Amer. Meteor. Soc.*, **98**, 495–501, <https://doi.org/10.1175/BAMS-D-16-0134.1>.
- , and E. Rappaport, 2000: Forecast skill of a simplified hurricane intensity prediction model. Preprints, *24th Conf. on Hurricanes and Tropical Meteorology*, Ft. Lauderdale, FL, Amer. Meteor. Soc., 236–237.
- , and D. Nolan, 2004: Tropical cyclone activity and global climate. *26th Conf. on Hurricanes and Tropical Meteorology*, Miami, FL, Amer. Meteor. Soc., 240–241.
- , C. DesAutels, C. Holloway, and R. Korty, 2004: Environmental control of tropical cyclone intensity. *J. Atmos. Sci.*, **61**, 843–858, [https://doi.org/10.1175/1520-0469\(2004\)061<0843:ECOTCI>2.0.CO;2](https://doi.org/10.1175/1520-0469(2004)061<0843:ECOTCI>2.0.CO;2).
- , S. Ravela, E. Vivant, and C. Risi, 2006: A statistical-deterministic approach to hurricane risk assessment. *Bull. Amer. Meteor. Soc.*, **87**, 299–314, <https://doi.org/10.1175/BAMS-87-3-299>.
- , R. Sundararajan, and J. Williams, 2008: Hurricanes and global warming: Results from downscaling IPCC AR4 simulations. *Bull. Amer. Meteor. Soc.*, **89**, 347–368, <https://doi.org/10.1175/BAMS-89-3-347>.
- , F. Fondriest, and J. Kossin, 2012: Potential economic value of seasonal hurricane forecasts. *Wea. Climate Soc.*, **4**, 110–117, <https://doi.org/10.1175/WCAS-D-11-00017.1>.

- Fedorov, A. V., C. M. Brierley, and K. Emanuel, 2010: Tropical cyclones and permanent El Niño in the early Pliocene epoch. *Nature*, **463**, 1066–1070, <https://doi.org/10.1038/nature08831>.
- Gaul, G. M., 2019: *The Geography of Risk: Epic Storms, Rising Seas, and the Cost of America's Coasts*. Farrar, Straus and Giroux, 304 pp.
- Gray, W. M., 1979: Hurricanes: Their formation, structure, and likely role in the tropical circulation. *Meteorology over the Tropical Oceans*, D. B. Shaw, Ed., Royal Meteorological Society, 155–218.
- Hourdin, F., and Coauthors, 2016: LMDZ6a: The atmospheric component of the IPSL climate model with improved and better tuned physics. *J. Adv. Model. Earth Syst.*, **12**, e2019MS001892, <https://doi.org/10.1029/2019ms001892>.
- Irvine, P., K. Emanuel, J. He, L. W. Horowitz, G. Vecchi, and D. Keith, 2019: Halving warming with idealized solar geoengineering moderates key climate hazards. *Nat. Climate Change*, **9**, 295–299, <https://doi.org/10.1038/s41558-019-0398-8>.
- Khairoutdinov, M. F., and K. Emanuel, 2013: Rotating radiative-convective equilibrium simulated by a cloud-resolving model. *J. Adv. Model. Earth Syst.*, **5**, 816–825, <https://doi.org/10.1002/2013MS000253>.
- Knapp, K. R., M. C. Kruk, D. H. Levinson, H. J. Diamond, and C. J. Neumann, 2010: The International Best Track Archive for Climate Stewardship (IBTrACS). *Bull. Amer. Meteor. Soc.*, **91**, 363–376, <https://doi.org/10.1175/2009BAMS2755.1>.
- Knutson, T., and Coauthors, 2019: Tropical cyclones and climate change assessment: Part I: Detection and attribution. *Bull. Amer. Meteor. Soc.*, **100**, 1987–2007, <https://doi.org/10.1175/BAMS-D-18-0189.1>.
- , and Coauthors, 2020: Tropical cyclones and climate change assessment: Part II: Projected response to anthropogenic warming. *Bull. Amer. Meteor. Soc.*, **101**, E303–E322, <https://doi.org/10.1175/BAMS-D-18-0194.1>.
- Kossin, J. P., 2018: A global slowdown of tropical-cyclone translation speed. *Nature*, **558**, 104–107, <https://doi.org/10.1038/s41586-018-0158-3>.
- , T. L. Olander, and K. R. Knapp, 2013: Trend analysis with a new global record of tropical cyclone intensity. *J. Climate*, **26**, 9960–9976, <https://doi.org/10.1175/JCLI-D-13-00262.1>.
- , K. A. Emanuel, and G. A. Vecchi, 2014: The poleward migration of the location of tropical cyclone maximum intensity. *Nature*, **509**, 349–352, <https://doi.org/10.1038/nature13278>.
- , —, and S. J. Camargo, 2016: Past and projected changes in western North Pacific tropical cyclone exposure. *J. Climate*, **29**, 5725–5739, <https://doi.org/10.1175/JCLI-D-16-0076.1>.
- Lee, C.-Y., S. J. Camargo, A. H. Sobel, and M. K. Tippett, 2020: Statistical–dynamical downscaling projections of tropical cyclone activity in a warming climate: Two diverging genesis scenarios. *J. Climate*, **33**, 4815–4834, <https://doi.org/10.1175/JCLI-D-19-0452.1>.
- Leipper, D. F., 1967: Observed ocean conditions and Hurricane Hilda, 1964. *J. Atmos. Sci.*, **24**, 182–186, [https://doi.org/10.1175/1520-0469\(1967\)024<0182:OOCANH>2.0.CO;2](https://doi.org/10.1175/1520-0469(1967)024<0182:OOCANH>2.0.CO;2).
- Liu, M., G. A. Vecchi, J. A. Smith, and H. Murakami, 2017: The present-day simulation and twenty-first-century projection of the climatology of extratropical transition in the North Atlantic. *J. Climate*, **30**, 2739–2756, <https://doi.org/10.1175/JCLI-D-16-0352.1>.
- Michaelis, A. C., and G. M. Lackmann, 2019: Climatological changes in the extratropical transition of tropical cyclones in high-resolution global simulations. *J. Climate*, **32**, 8733–8753, <https://doi.org/10.1175/JCLI-D-19-0259.1>.
- Montgomery, M. T., and R. K. Smith, 2012: The genesis of Typhoon Nuri as observed during the tropical cyclone structure 2008 (TCS08) field experiment. Part 2: Observations of the convective environment. *Atmos. Chem. Phys.*, **12**, 4001–4009, <https://doi.org/10.5194/acp-12-4001-2012>.
- Müller, W. A., and Coauthors, 2018: A higher-resolution version of the Max Planck Institute Earth system model (MPI-ESM1.2-HR). *J. Adv. Model. Earth Syst.*, **10**, 1383–1413, <https://doi.org/10.1029/2017MS001217>.
- Murakami, H., and Coauthors, 2015: Simulation and prediction of category 4 and 5 hurricanes in the high-resolution GFDL HiFLOR coupled climate model. *J. Climate*, **28**, 9058–9079, <https://doi.org/10.1175/JCLI-D-15-0216.1>.
- , T. L. Delworth, W. F. Cooke, M. Zhao, B. Xiang, and P.-C. Hsu, 2020: Detected climatic change in global distribution of tropical cyclones. *Proc. Natl. Acad. Sci. USA*, **117**, 706–714, <https://doi.org/10.1073/pnas.1922500117>.
- Olander, T. L., and C. S. Velden, 2019: The advanced Dvorak technique (ADT) for estimating tropical cyclone intensity: Update and new capabilities. *Wea. Forecasting*, **34**, 905–922, <https://doi.org/10.1175/WAF-D-19-0007.1>.
- Patricola, C. M., R. Saravanan, and P. Chang, 2018: The response of Atlantic tropical cyclones to suppression of African easterly waves. *Geophys. Res. Lett.*, **45**, 471–479, <https://doi.org/10.1002/2017GL076081>.
- Price, J. F., 1981: Upper ocean response to a hurricane. *J. Phys. Oceanogr.*, **11**, 153–175, [https://doi.org/10.1175/1520-0485\(1981\)011<0153:UORTAH>2.0.CO;2](https://doi.org/10.1175/1520-0485(1981)011<0153:UORTAH>2.0.CO;2).
- Raavi, P. H., and K. J. E. Walsh, 2020: Sensitivity of tropical cyclone formation to resolution-dependent and independent tracking schemes in high-resolution climate model simulations. *Earth Space Sci.*, **7**, e2019EA000906, <https://doi.org/10.1029/2019EA000906>.
- Roberts, M. J., and Coauthors, 2020: Projected future changes in tropical cyclones using the CMIP6 HighResMIP multi-model ensemble. *Geophys. Res. Lett.*, **47**, e2020GL088662, <https://doi.org/10.1029/2020gl088662>.
- Rotunno, R., Y. Chen, W. Wang, C. Davis, J. Dudhia, and C. L. Holland, 2009: Large-eddy simulation of an idealized tropical cyclone. *Bull. Amer. Meteor. Soc.*, **90**, 1783–1788, <https://doi.org/10.1175/2009BAMS2884.1>.
- Sellar, A. A., and Coauthors, 2020: Implementation of U.K. Earth system models for CMIP6. *J. Adv. Model. Earth Syst.*, **12**, e2019MS001946, <https://doi.org/10.1029/2019ms001946>.
- Sugi, M., Y. Yamada, K. Yoshida, R. Mizuta, M. Nakano, C. Kodama, and M. Satoh, 2020: Future changes in the global frequency of tropical cyclone seeds. *SOLA*, **16**, 70–74, <https://doi.org/10.2151/SOLA.2020-012>.
- Swart, N. C., and Coauthors, 2019: The Canadian Earth System Model version 5 (CanESM5.0.3). *Geosci. Model Dev.*, **12**, 4823–4873, <https://doi.org/10.5194/gmd-12-4823-2019>.
- Tang, B., and S. J. Camargo, 2014: Environmental control of tropical cyclones in CMIP5: A ventilation perspective. *J. Adv. Model. Earth Syst.*, **6**, 115–128, <https://doi.org/10.1002/2013MS000294>.
- Tatebe, H., and Coauthors, 2019: Description and basic evaluation of simulated mean state, internal variability, and climate sensitivity in MIROC6. *Geosci. Model Dev.*, **12**, 2727–2765, <https://doi.org/10.5194/gmd-12-2727-2019>.
- Tippett, M. K., S. Camargo, and A. H. Sobel, 2011: A Poisson regression index for tropical cyclone genesis and the role of large-scale vorticity in genesis. *J. Climate*, **24**, 2335–2357, <https://doi.org/10.1175/2010JCLI3811.1>.

- Vecchi, G. A., and Coauthors, 2019: Tropical cyclone sensitivities to CO<sub>2</sub> doubling: Roles of atmospheric resolution, synoptic variability and background climate changes. *Climate Dyn.*, **53**, 5999–6033, <https://doi.org/10.1007/s00382-019-04913-y>.
- Vitart, F., and Coauthors, 2007: Dynamically-based seasonal forecasts of Atlantic tropical storm activity issued in June by EUROSIP. *Geophys. Res. Lett.*, **34**, L16815, <https://doi.org/10.1029/2007GL030740>.
- Voldoire, A., and Coauthors, 2019: Evaluation of CMIP6 deck experiments with CNRM-CM6-1. *J. Adv. Model. Earth Syst.*, **11**, 2177–2213, <https://doi.org/10.1029/2019MS001683>.
- Walsh, K., M. Fiorino, C. W. Landsea, and K. L. McInnes, 2007: Objectively determined resolution-dependent threshold criteria for the detection of tropical cyclones in climate models and reanalyses. *J. Climate*, **20**, 2307–2314, <https://doi.org/10.1175/JCLI4074.1>.
- Wing, A. A., K. Emanuel, C. E. Holloway, and C. Muller, 2017: Convective self-aggregation in numerical simulations: A review. *Surv. Geophys.*, **38**, 1173–1197, <https://doi.org/10.1007/s10712-017-9408-4>.
- Yamaguchi, M., J. C. L. Chan, I.-J. Moon, K. Yoshida, and R. Mizuta, 2020: Global warming changes tropical cyclone translation speed. *Nat. Commun.*, **11**, 47, <https://doi.org/10.1038/s41467-019-13902-y>.
- Zhang, G., H. Murakami, T. R. Knutson, R. Mizuta, and K. Yoshida, 2020: Tropical cyclone motion in a changing climate. *Sci. Adv.*, **6**, eaz7610, <https://doi.org/10.1126/sciadv.aaz7610>.